Materials Horizons

From Stress to Charge: Investigating the Piezoelectric Response of Solvate Ionic Liquid in Structural Energy Storage Composites

Journal:	*Materials Horizons*
Manuscript ID	MH-COM-05-2024-000612.R1
Article Type:	Communication
Date Submitted by the Author:	23-Jul-2024
Complete List of Authors:	Henderson, Luke; Deakin University, Institute for frontier materials Dharmasiri, Bhagya; Deakin University, IFM Simon, Žan; Deakin University, Institute for frontier materials Harte, Timothy; Deakin University, Institute for Frontier Materials Sherrell, Peter; RMIT University

New Concepts Statement

We report the piezoelectric response of a solvate ionic liquid (SIL), consisting of lithium bis(trifluoromethanesulfonyl)imide (LiTFSI) solvated by triethylene glycol dimethyl ether (G3); a characteristic never observed in this liquid-at-room-temperature salt in its solvated form. SIL's are seeing a rapid uptake in energy storage due to their highly desirable properties such as broad thermal and chemical stability. A piezoelectric effect was recently discovered in pure ionic liquids, followed by a qualitative analysis and demonstration of the underlining liquid-to-crystalline phase conversion following pressurisation and depressurisation. The electromechanical responsiveness following applied stress was investigated in [Li-G3]TFSI, as well as a part solid polymer electrolyte commonly used in energy storage devices. Carbon fibre-based supercapacitors are multifunctional materials that can be used in load-bearing applications whilst supporting charge transfer and storage reactions. Novel applications for these liquids in composite electrochemical devices rely on their piezoelectric properties to complement traditional charge processes through layered ordering of SIL chains, thus improving efficiency without adding to weight. The observed phenomena suggest that SILs can act as smart materials, responding to mechanical stimuli following direct a piezoelectric effect. This characteristic could be harnessed to develop innovative, efficient, and safe energy storage composites.

From Stress to Charge: Investigating the Piezoelectric Response of Solvate Ionic Liquid in Structural Energy Storage Composites

Simon, Žan[1], Dharmasiri, Bhagya[1], Harte, Timothy[1], Sherrell, Peter C.[2], Henderson, Luke C.[1]*

[1]Institute for Frontier Materials, Deakin University, Waurn Ponds, VIC 3216 Australia

[2]School of Science, RMIT University, Melbourne, VIC 3000 Australia

*Corresponding author email: luke.henderson@deakin.edu.au

Abstract

Solvate ionic liquids (SILs) are a class of ionic liquids where the liquid-state salt is chelated by a coordinating solvent, and of interest due to their advantageous properties such as low vapour pressure and superb thermal and chemical stability for energy storage applications. The electromechanical and piezoelectric effect were studied in lithium bis(trifluoromethanesulfonyl)imide (LiTFSI) solvated by triethylene glycol dimethyl ether (triglyme, G3), forming [Li-G3]TFSI. These effects were also investigated in full solid polymer electrolyte (SPE) used in energy storage devices, consisting of [Li-G3]TFSI paired with an epoxy-based resin system. The SIL's electromechanical response was first established in isolation, as well as within the SPE. Experimental data demonstrates the effect of a major part of the SPE contributing to the electrical potential generation during application of force and subsequent pressurisation as well as depressurisation, underlined by a direct piezoelectric effect. SPE response to applied load is explored after recent discovery of liquid-to-crystalline phase transition following pressurisation in pure ionic liquids. This finding has the potential to ameliorate the performance of energy storage composites via additional effects of charging such as device by subjecting it to stress, leading to increased efficiency. Results to date show a bulk potential difference across the SIL of up to 150 mV, while the SPE potential response is scaled down due to significantly lower volume of SIL at the interface (~30 mV). Nevertheless, such findings can still significantly affect the performance of carbon fibre (CF)-based structural supercapacitors and batteries that are able to store and release electrical energy whilst simultaneously contributing to load-bearing performance.

Keywords:

Solvate ionic liquids, ionic liquids, piezoelectric effect, solid polymer electrolytes

1 Introduction

Solvate ionic liquids (SILs) are a subset of ionic liquids (ILs), where the traditional chemical composition is altered by the incorporation of cationic hosts (typically oligoethers).[1] The typical SIL structure includes chelated alkali metal cation such as lithium, with a coordinated ether-based solvent, creating a charge diffuse cation, and a similarly soft counterion.[2] In addition to offering the same advantages as traditional ILs in terms of their high ionic conductivity, wide electrochemical window, near-zero vapour pressure, and thermal stability, SILs obviate some of the limitations associated with traditional ILs, namely their chemical instability, presence of impurities derived from multistep synthesis, prohibitive cost, and less efficient ion transport.[3-7] Due to this hybrid system where additional properties are derived from the polyether, an additional dimension enables fine tuning for specific applications such as electrolytes for alkali metal ion batteries and supercapacitors.[8, 9] Unique properties of SILs include high resistance to electrochemical oxidation of the cation complex due to attenuation of the highest occupied molecular orbital (HOMO) energy level of oligo-glyme through complexation with lithium,[9, 10] lithium transport *via* ligand exchange, as well as lithium acceleration (*i.e.* autonomous and rapid movement of lithium in contrast with oligo-glyme and anion constituents).[11]

When combining these SILs with a thermoset resin system, ionic gels are formed.[12, 13] In these ternary solid polymer electrolytes (SPEs), SILs also act as a plasticising agent and facilitator of fast ion transport, *via* their decoupling from the segmental motion of the polymer.[14] These SPEs also display lower ionic conductivity but higher Young's modulus with low SIL content and vice versa with respect to pure SIL.[15] However, this inverse relationship is not proportional, with marginal improvements in mechanical properties following a reduction of SIL content down to 50% w/w.[16] Nevertheless, this trade-off and focus on property enhancement is the main driver in selection of SIL proportion within a thermoset polymer system, with 70% w/w being prominent in literature.[17-20]

A recent study evaluated a flexible structural supercapacitor (SSC) device encapsulated in an SPE based on bicontinuous SIL/epoxy resin system using surface-functionalised CF as electrodes (Fig. 2-G-i), grafted with conductive and redox-active poly(*o*-phenylenediamine), resulting in significant pseudocapacitive improvements.[17] A large change in capacitance was observed when device was subjected to deformation at varying angles, with the largest capacitive enhancement observed at angles between 90° and 135°. This capacitance then reverted to original value when device was returned to its flat form. The mechanism for this enhancement was unknown and thus of interest for further exploration.

Recent work of Hossain *et al.*[21] demonstrated a piezoelectric effect in ionic liquids *via* the application of pressure. Subsequent in-depth investigations from Hossain *et al.*[22] then revealed the mechanism behind this direct piezoelectric effect and attributed it to a liquid-to-crystalline phase transition in response to the applied pressure, observed via high-pressure X-ray diffraction (XRD). We hypothesised that this piezoelectric response is resulting from the compression and tension of the SIL within the polymer electrolyte, may be providing an additive contribution to the higher specific capacitance. To test this hypothesis, it had to be determined if the SILs used in the polymer electrolytes in the previously described SSCs also displayed this piezoelectric phenomenon, and if so, on what scale and how reliably. Moreover, if this unusual effect is observed for SILs, does it translate to a polymer electrolyte blend. However, the use of a neat ionic liquid in such a system to harvest energy is difficult to imagine. Whereas the incorporation of these piezo-responsive liquids into a polymer may provide a simple and convenient means to manipulate these substances for energy harvesting.

In this work, we show that it is not only possible to harvest energy from a pure SIL, but also from a biphasic system of SIL and epoxy resin, bringing the possibility of incorporation of electromechanical responsive liquids to the composites space. Typical composite structure involves a reinforcing fibre (*e.g.* carbon fibre), within a matrix that is often a thermosetting resin. Proposed focus should therefore be turned to enabling multifunctional materials and further research into 'mass-less' structural energy storage, as well as practical uses in industries such as renewable energy, electric vehicles, and aerospace. Such a transient piezoelectric effect can enable faster charging structural electrochemical devices in the future and providing greater energy density of charge storage devices within the same footprint. Furthermore, it can guide manufacture of devices, whose tailored design and physicochemical impact of the tuneable liquid components on their performance, govern more efficient electrochemical devices in the future *via* self-charging capabilities, as well as enabling pathways for structural health monitoring applications, and enhanced sensitivity of existing pressure sensors.

2 Experimental Methods

2.1 Synthesis of SILs

All chemicals and solvents were purchased from Sigma-Aldrich Australia (Merck Group, United States) and used without further purification. RIM935 epoxy resin and RIM936 hardener were obtained from Ironbark Composites (Australia). [Li-G3]TFSI was synthesised according to previously published reports,[11] combining triethylene glycol dimethyl ether (G3 or triglyme) with lithium bis-(trifluoromethanesulfonyl)imide (LiTFSI) at a molar ratio of 1 to 1.5, providing 2.67 ether oxygen atoms

per lithium atom (Fig. 1-A). Reactants were stirred at room temperature for two days and subsequently dried under high vacuum, stirring for 1 h at 140 °C to remove any residual water.

2.2 Compression and OCP Measurements

Aluminium cylinder was manufactured with a tight-fitting plunger (Fig. 1-A). Aluminium rods were parted off and resurfaced on a Wabeco D6000 (Walter Blombach GmbH, Germany) metal lathe. Rod was then drilled into, leaving a 30 mm recess, and the inside diameter increased to 15.22±0.04 mm using a boring bar with HSS steel to ensure a liquid tight, but not airtight seal with the additively manufactured plunger made from polylactic acid (PLA) on ISO 52900 material extrusion (MEX) 3D printing machine Prusa i3 Mk4 (Prusa Research, Czech Republic). A slot was manufactured to accept a rubber seal on the end, ensuring tighter fit. Copper wire (r = 0.5 mm), serving as the electrode, was attached to the bottom of the cylinder, and coated with an 8331D - Silver Conductive Epoxy Adhesive (M.G. Chemicals, Canada) to ensure good contact with the aluminium cylinder. Another piece of copper wire (r = 0.5 mm) was inserted through the PLA plunger, ensuring contact with the IL during compression. Cyclic compressive testing was performed on an Instron universal testing system series 5967 load frame, fitted with a 1 kN load cell (Illinois Tool Works Inc., United States). Upon application of compressive loads of up to 3.3 MPa, open circuit potential (OCP) was monitored within the cylinder and recorded with the Autolab PGSTAT204 portable potentiostat (Metrohm, Switzerland) at a sampling rate of 40 S/s. Increasing force was applied in duplicates, followed by two rounds of lower initial force. Displacement rate of 5 mm/s was used throughout the study to ensure quick pressurisation. A constant pre-load of 2.5 N prevented contact electrification effects between surfaces.

2.3 Bicontinuous Electrolyte Preparation

Synthesis was published previously and full characterisation was also performed.[16] Briefly, synthesised [Li-G3]TFSI (1:1.5) was mixed with RIM935/936H epoxy resin system in a 7:3 ratio by adding non-degassed, pre-mixed resin and hardener into the SIL and thoroughly mixing. Since SIL significantly shortens cure times,[23] with this particular SPE formulation seeing an 88.5% reduction in gel-time,[16] SPE was poured directly into the aluminium cylinder and kept for 72 hours in a desiccator prior to testing to ensure full cure.

2.4 Scanning Electron Microscopy (SEM)

SEM was used to study the surface morphology of SPE to characterize its nano- and mesoporous structure (Fig. 2-A). The samples were first prepared on a CUT 5062 rotary microtome (SLEE medical GmbH, Germany) to obtain thin slices with a thickness of 50 µm. These were then sputter coated with

a Leica EM ACE600 (Leica Microsystems, Germany) using 5 nm thick gold sputtering, and imaged using a field emission scanning electron microscope JSM-7800F (JEOL Ltd., Japan) at 3 keV.

3 Results and Discussion

Of initial focus was to determine if the neat SILs displayed a similar piezoelectric effect as those reported by Hossein *et al.*[21] as the SILs were not part of their study. Our testing apparatus needed significant optimisation to ensure the plunger allowed gaseous headspace passage without SIL leakage under pressure. To achieve this, the SIL's viscosity was increased by adding a super-stoichiometric amount of LiTFSI in a 1.5:1 ratio with triglyme.[11]

When evaluated as the neat SIL, a consistent potential response was observed with the application of pressure. A wide range of forces (250-600 N; 1.37-3.30 MPa) was first applied, resulting in a consistent OCP output of around 150 mV (Fig. 1-B). The application of increasing forces to the SIL in smaller step sizes showed a distinct and proportional increase in electrical potential output (Fig. 1-C), though the authors considered that the systematic increase in potential may be due to the accumulation of charge from previous pressure applications. Therefore, after a series of pressures was applied to the SIL, a significantly reduced load was applied (Fig. 1-C, dashed vertical line), correlating to a proportionally smaller potential response. It was observed that the output reduced from 95 mV to 39 mV when the force was reduced from 197 N (1.08 MPa) to 56 N (0.31 MPa). This behaviour aligns with Hossain *et al.*[22], suggesting that the SIL crystallises within the polymer under pressure and reverts to a solution when pressure is removed. Thus, the output appears related to the degree of crystallisation. At forces exceeding 200 N (1.10 MPa) up to 600 N (3.30 MPa), the OCP response plateaued around 150 mV (Fig. 1-B), indicating a pressure limit to the generated potential when induced crystallisation reaches saturation under these test conditions.

These results show a lower OCP magnitude (197 N, 95 mV), compared with Hossain *et al.*[21, 22] (*e.g.* 200 N, 3,380 mV). This discrepancy is attributed to (i) solvated nature of the SIL *vs.* pure IL and (ii) differences in volume used (200 µL *vs.* 5 mL) that results in considerable variations in resistance. However, the transient phase transition effect remains the same. Using a lower volume increases electrical potential due to an interface-dominated response,[24] which is significantly larger than the bulk potential observed with 5 mL, corresponding to a 25x volume increase.

Individual waveforms (Fig. 1-D) show the OCP response to pressurisation (first peak) and depressurisation (second, smaller peak). The depressurisation during the retract phase, corresponding to a negative applied force, results in a positive measured potential. Studies have shown some ILs can form crystal structures under pressure,[25] with some only displaying crystal polymorphism during

decompression,[26] or a combination of both. The evolution of OCP over time and pressure stimulus shows a clear compression and decompression peak. This suggests that [Li-G3]TFSI responds to both pressurisation and depressurisation steps, and is proportionally pressure-dependent at approximately 4.8 mV per every 10 N of applied force, R^2 = 0.97304 (Fig. 1-E).

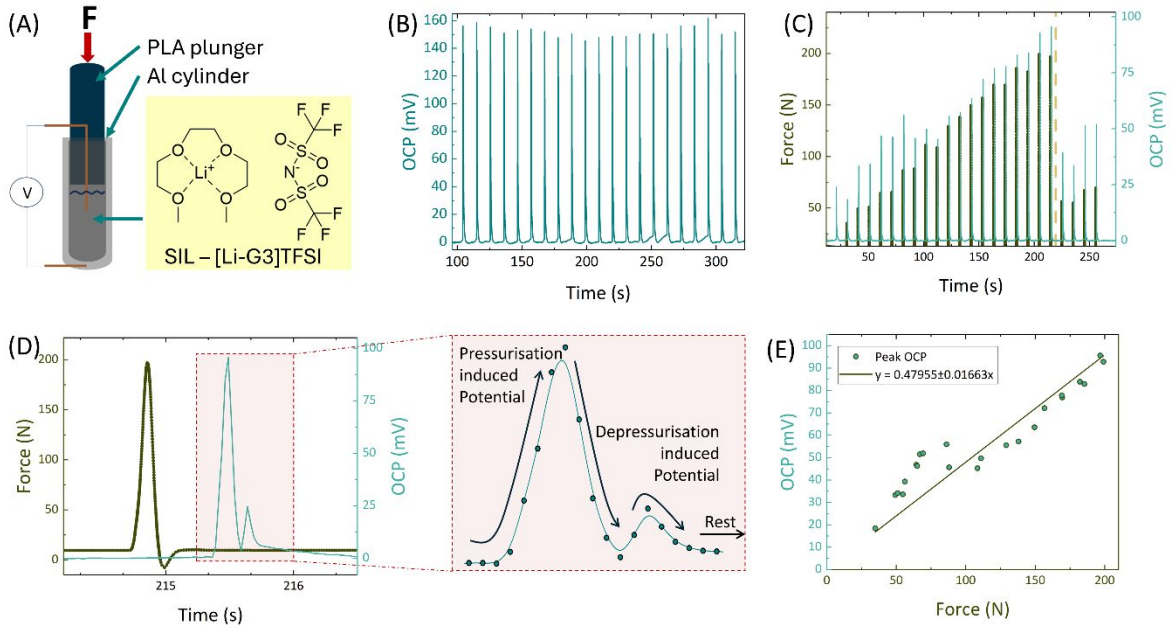

Fig. 1. *A) Schematic representation of the internal components of the testing apparatus linked to a potentiostat via copper wire (in orange), and showing the liquid component's SIL structure; B) OCP plot as a function of time, compressing the SIL at 250-600 N (1.37-3.30 MPa); C) Dual y-axis plot of applied force (olive green) and OCP (cyan) as a function of time, compressing the SIL at increasing force in duplicates, two rounds of lower initial force (past dashed vertical line), and displacement of 5 mm/s, with a pre-load of 2.5 N; D) OCP plot as a function of time, focusing on one representative event (force/OCP pair) from* ***C*** *and an inset schematic of events occurring during one OCP response overlayed on scatter point data; E) Scatter plot of OCP response (cyan) as a function of applied force (olive green), showing a linear relationship via fitted model,* R^2 *= 0.97304.*

When the SPE, a bicontinuous electrolyte consisting of SIL and epoxy resin, was subjected to a similar compression testing, an OCP response was observed (Fig. 2-B). Albeit at a smaller scale with a 3x smaller response generated (noting the SPE was more compressible than pure SIL). This is likely due to the reduced amount of ionic liquid present within the testing chamber and at the interface, as it comprises 70% of the polymer-SIL mixture (Fig. 2-A, top surface). It is also possible that within the porous polymer network some pockets of SIL may not connect within the bicontinuous phase and therefore do not contribute to the final potential output, thus suppressing the observed response.

An unusual peak shape was observed in the SPE testing waveform (Fig. 2-D), showing a second small spike after initial pressurisation and depressurisation. This second peak, occurring about 0.2 seconds after maximum potential response, likely correlates to plunger recession. This may also indicate a delayed SIL continuous-phase reorganisation within the mesopore structure. Since the SPE is more compressible than pure SIL, energy absorption also plays a role in pressure dissipation, thus resulting in lower effective (operating) pressure SIL within the SPE is experiencing. SPE exhibits the complex waveform of OCP as during depressurisation/release the epoxy phase rebounds, inducing turbulent flow and resulting in 2nd order charge effects.

As expected, an asymptotic fit of the scatter plot of peak-to-peak OCP as a function of force suggests a pressure limit to the degree of generated electrical potential when the amount of induced crystallisation reaches a saturation point under these test conditions (Fig. 2-C). A linear pressure-dependence was not observed at the selected pressures and is thought to occur at much lower pressures when applied force is below 20 N. Similarly, pure SIL also reached such OCP plateau, however only above 250 N (1.37 MPa) (Fig. 1-B) due to inherent differences in relative amount of SIL undergoing piezoelectric effect when comparing pure SIL and SPE.

To deconvolute the OCP responses between applied stress and its release, a 2-second hold was introduced to the applied force. Figure 2-E shows the response of neat SIL, with only two representative events plotted for clarity. Of note, similar trends in waveform shape and OCP progression over time was observed with SPE (Fig. 2-F), enabling translation of the phase-transitory effects from neat SIL to the SPE. From a fluid dynamics perspective, a pressurised hold of two seconds enables separation of peaks that contribute to the total OCP response of one cycle with a turbulent-stationary-turbulent flow pattern. The applied pressure resulted in fluid flow that is a competition between interactions in the liquid phase and at the fluid/solid body interface, leading to shearing at the weakest interface.[27] However, no direct relationship between friction and turbulent flow during shearing was found. Displacement of the plunger during compression testing of SIL was on the scale of 0.44±0.14 mm, with the 2-second hold for SIL testing showing a displacement of 0.44±0.13 mm. Nevertheless, the bulk of change in displacement with SIL testing can be attributed to the elastomer seal used on the plunger, so pressure-induced crystallisation would still be considered the main contributor to the OCP response as opposed to flow-induced friction against the confinement walls of the aluminium cylinder. Events occurring during the 2-second hold testing of pure SIL show a clear double peak response (Fig. 2-E), in the same manner as before without the 2-second hold (Fig. 1-D).

The SPE showed larger displacement (0.78±0.32 mm) and even greater with a 2-second hold (0.90±0.31 mm), indicating higher compressibility and complex OCP waveforms due to 2nd order

charge effects during epoxy phase depressurisation. The 2-second hold allows equilibrium, eliminating this effect (Fig. 2-F). The SPE voltage equilibrates faster with less SIL ordering and smaller pore volume, leading to less flow/convection and sharper features (Fig. 2-F) compared to broader peaks (Fig. 2-E). This is due to the epoxy phase absorbing compressive load off the incompressible SIL.

Previous studies have investigated the phase behaviour of ILs under pressure. Yoshimura *et al.*[25] observed vibrational changes in the CH stretching spectrum above 4 GPa, without crystallisation up to 5.5 GPa. Takekiyo *et al.*[28] and Su *et al.*[29] observed pressure-induced partial crystallisation in different ILs. These findings therefore suggest that the liquid-to-crystalline phase transition and piezoelectric effect in ILs are pressure-dependent and linked to molecular structure. Various techniques, including small-angle X-ray scattering, have revealed structural changes in pressurised ILs, particularly when pressurised with gases like carbon dioxide.[30] Multiple phase transitions and crystallisation under extreme pressure conditions have been detected, indicating that phase-change induced potential response is possible, but transient.[26, 29] Moreover, applying pressure to a liquid in a confined space can result in structural changes and modifications in the friction force and electric field within a confined system, and it is also heavily dependent on the fluid's molecular structure.[31] An increase in applied pressure can lead to changes in the ILs viscosity, density, and flow patterns, with liquids possibly exhibiting non-Newtonian behaviour. Due to spatial restriction in confined environments, ILs interact strongly with solid surfaces (*i.e.* in this instance plunger and cylinder aluminium walls) which has a pronounced effect on their phase transition behaviour, molecular organisation near surface walls, wetting ability, and ionic interactions.[32]

SIL usage within nano- and mesoporous matrices enable integration of their properties into soft polymers, whilst providing structural support for more efficient ion-transfer at longer distances (*e.g.* across the dielectric separator in energy storage devices). SILs prevent the solid network from collapsing onto itself during its rapid cure,[23] while the network confines the IL in order to ensure its consistent function.[32]

Similar SIL-infused SPEs have been effectively used in structural energy storage composites, utilising CF electrodes and glass fibre separators (Fig. 2-G-i). When subjected to deformation, such as bending, the CF electrodes inside the bend point experience compressive forces, while those on the outside face tensile forces (Fig. 2-G-ii). This dual-force scenario creates a unique environment for the nanoconfined SIL within the SPE. The SIL, confined within the pores of the SPE, undergoes compression from both the CF electrodes at the interface and the surrounding SPE's epoxy matrix. This compression impacts the SIL's structural and electrical properties. Due to the continuous nature of the SIL phase and its inherent ionic conductivity, these mechanical deformations induce a transient piezoelectric

effect, generating potential differences. This critical phenomenon enables detection and harnessing of electrical potential from mechanical strain. Detecting these potential differences can enhance structural energy storage devices, converting deformation into usable electrical energy (Fig. 2-G). This integration of mechanical responsiveness and energy storage advances the development of multifunctional materials and devices.

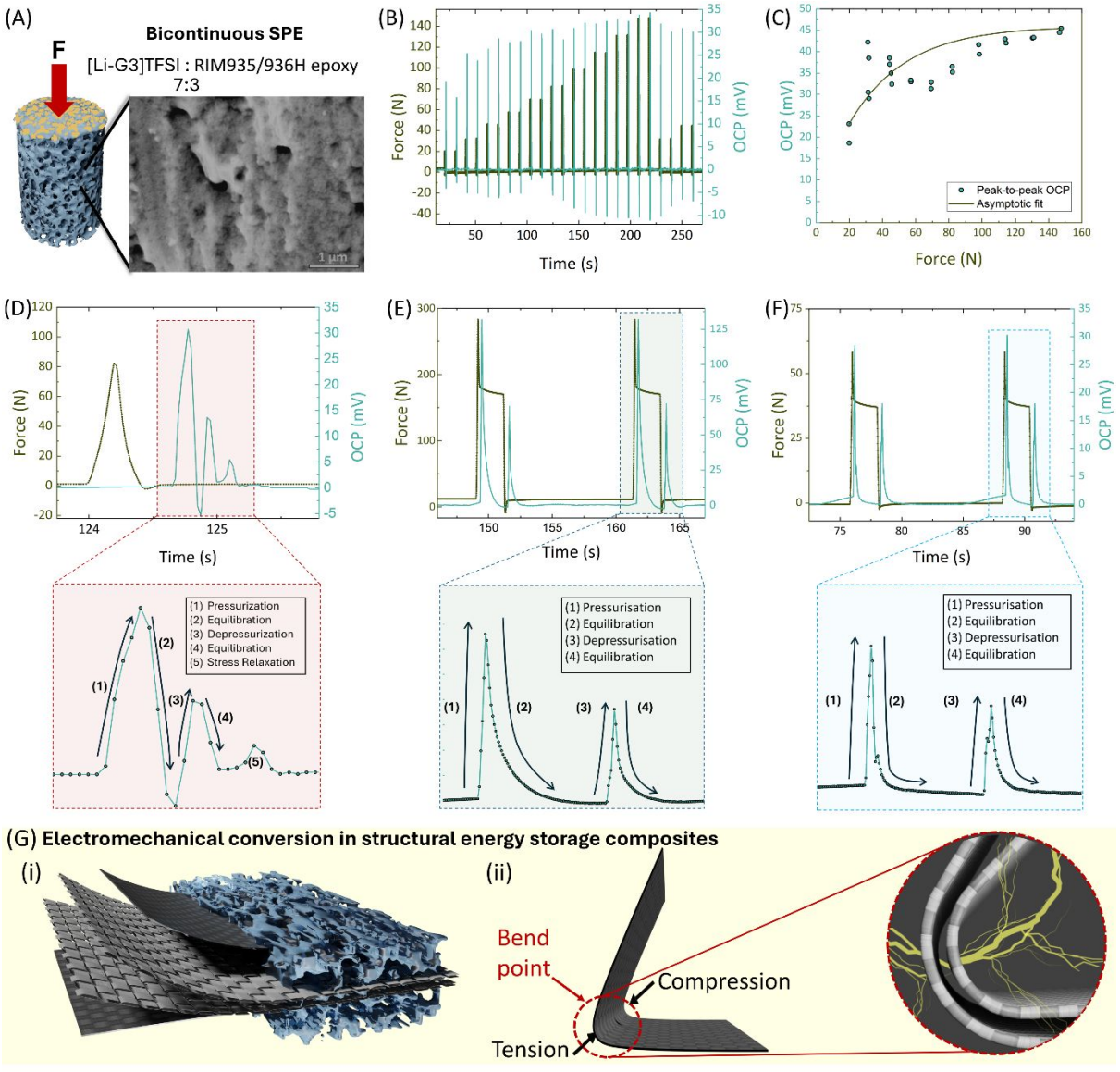

Fig. 2. *A) Schematic representation of porous bicontinuous solid polymer electrolyte, with an inset figure of an SEM image showing surface topography; B) Dual y-axis plot of applied force (olive green) and OCP (cyan) as a function of time, compressing the SPE at increasing force in duplicates, two rounds of lower initial force, and displacement of 5 mm/s, with a constant pre-load of 2.5 N; C) Scatter plot of OCP response (cyan) as a function of applied force (olive green), showing an exponential asymptotic relationship via fitted model,* $R^2 = 0.37103$*, reaching a pressure limit to the SPE in this system; D) OCP*

*plot as a function of time, focusing on one representative event (force/OCP pair) from **B**; E) Dual y-axis plot of applied force (olive green) and OCP (cyan) as a function of time, showing two events of the whole test procedure for clarity, compressing the SIL; F) Dual y-axis plot of applied force (olive green) and OCP (cyan) as a function of time, showing only two events of the whole test procedure for clarity, compressing the SPE. All inset schematics are showing events occurring during one OCP response overlayed on scatter point data; G-i) Structural supercapacitor (SSC) showing the layup of CF-based supercapacitor; G-ii) SSC being bent with direction of tension and compression forces, with the inset figure showing the difference in thickness at the bend point (i.e. layers coming closer together at bend point only).*

This structure organisation due to ion-paired dipolar species in highly organised stacks was observed by others as well, with the structure spanning anywhere between several nm to 1 µm.[33-36] Piezoelectric response is also further complicated by the fact that ILs undergo stable and ordered structuring and generate significant endogenous electric fields that last for prolonged periods of time following the removal of external potential.[37] This electric field is responsible for the increasing OCP, and a need to baseline subtract the data becomes necessary when comparing OCP response to applied stress. This general upwards trend in OCP was also observed by Hossain *et al.*[21] Additionally, microstructure of dielectric and electrode materials and their interactions at the interface level can be significantly tweaked by the internal electric field formation.[38] Using a piezoelectric separator and mechanically responsive electrolyte, with the latter being explored by this study, can have profound effect on the direction and magnitude of such an electric field, ultimately impacting performance and output of the final device by enabling faster charging structural electrochemical devices in the future.

Research has shown that liquid-to-solid contact electrification can generate charge *via* electron transfer when contacted with a hydrophobic solid surface (*i.e.* rubber seal used in compressive testing setup).[39] In ILs, contact electrification was also investigated and found to contribute to charging, but *via* ion transfer instead, where periodic contacting was able to reach a power density of up to 0.12 mW/m^2.[40] However, these effects did not apply to our system due to (i) fully contacting the sample and (ii) running a stabilisation run for charge dissipation by contacting and running 30 compressive cycles before data collection presented above.

Efficiently detecting piezoelectricity and harvesting energy from these unconventional sources (*i.e.* liquids) remains a significant challenge, with confounding effects greater when trying to establish their role within full composites. Piezoelectric materials' ability to convert mechanical stress into electrical energy offers a means to capture energy from a variety of ambient sources, such as vibrations, pressure fluctuations, or even sound waves. Inclusion of piezoelectric elements within a matrix can

lead to discovery of novel energy harvesting devices capable of harnessing energy from diverse sources, such as ocean waves, wind, or human motion. The converse piezoelectric effect, where an applied electric field induces mechanical strain, can also be exploited. 'Smart' energy storage devices could potentially convert electrical energy into pressure or vibrations, offering functionalities beyond simple energy storage, such as an electric vehicle braking system. Utilising a regenerative braking mechanism with IL-based braking fluid, the electric motor could be used to generate an electric field within the electrolyte, inducing a mechanical strain in the system. This strain could then be utilized to capture the braking energy more efficiently and improving the overall vehicle range. Combining SIL effects with piezoelectric separators opens new opportunities for improving power and energy density of structural energy storage composites. Piezoelectric elements have already been used to charge an activated-carbon-based supercapacitor,[41] however such an electrode cannot be considered a load carrying structural material. CFs are therefore a notable candidate, enabling production of multifunctional devices due to their simultaneous conductivity and excellent load-bearing abilities. Research avenues include CF use for shape-conforming *in-situ* strain sensor, structural health monitoring, kinetic energy harvesting in composites and much more.[42, 43]

4 Conclusion

Within the energy storage space SILs have seen widespread use as a major component in electrolytes due to their highly desirable properties and tuneable nature. Phase-shifting behaviour of SILs in high pressure environments has been explored, with results showing that [Li-G3]TFSI follows the same mechanism and is able to generate a voltage difference *via* its transient crystalline arrangement being highly responsive to mechanical stress. Their ability to undergo structural transitions when subjected to external forces opens new avenues for the design of advanced energy storage devices. SILs have also been shown to undergo liquid-to-crystalline phase transition when confined in the nano- and mesoporous structure of SPE used in structural supercapacitors, with stark changes to their properties such as ionic mobility and viscosity. Despite numerous factors affecting results such as degree of wetting of pores within matrix, leakage due to viscosity changes under nano-confinement, as well as general inaccessibility to surface characterisation techniques, there are clear correlations with stress-induced formation of crystalline structure and piezoelectric response of both SIL and SPE. Observed phenomena suggest that SIL can act as smart materials that respond to mechanical stimuli, enabling the conversion of mechanical energy into electrical energy following direct piezoelectric effect. This characteristic could be harnessed to develop innovative energy storage systems that are more efficient, safer, and environmentally friendly compared to current technologies. Developing cost-effective and scalable production methods is crucial when moving into composites space. Additionally,

the long-term stability and compatibility of SILs with supercapacitors and battery electrode materials need further investigation, ensuring minimal degradation of both as well as focus on device recyclability. Future research should focus on optimising the composition and confinement conditions of SILs to maximise their energy storage capabilities and on integrating these materials into practical devices.

CRediT Authorship Contribution Statement

Žan Simon: Conceptualisation, Methodology, Validation, Data Curation, Formal analysis, Investigation, Writing – original draft, Writing – review & editing, Visualisation. **Bhagya Dharmasiri:** Investigation, Supervision, Validation, Writing – Original Draft, Writing – Review & Editing. **Timothy Harte:** Methodology, Investigation, Resources, Data Curation. **Peter C. Sherrell:** Conceptualisation, Formal analysis, Visualisation, Writing – Review & Editing. **Luke C. Henderson:** Conceptualisation, Visualisation, Writing – Review & Editing, Supervision, Funding acquisition, Project administration.

Data Availability

The raw data is available via our university repository.

Ž. Simon, B. Dharmasiri, T. Harte, Timothy, P. C. Sherrell, L. C. Henderson, 2024, Deakin University Research Repository, DOI: https://doi.org/10.26187/deakin.c.7362889

Conflicts of Interest

The authors declare that they have no known competing financial interests or personal relationships that could have appeared to influence the work reported in this paper.

Acknowledgements

The authors gratefully acknowledge the support and contributions from Deakin University, the Australian Research Council (ARC) through the Discovery Programme (DP220100130), via the ARC Mid-Career industry fellowship scheme (IM230100048) and collaborators at RMIT and University of Melbourne, particularly within Peter Sherrell's research group. Special appreciation is extended to the Office of Naval Research Global [N62909-22-1-2052] for their invaluable support in this endeavour. Authors would also like to thank Australian National Fabrication Facility (ANFF) – Victoria, for facilitating use of vital equipment. The investigation took place at the facilities of the Institute for

Frontier Materials and Carbon Nexus at Deakin University, where vital resources and excellent technical support were made available, contributing significantly to the successful execution of this study.

References

1. C. Austen Angell, Y. Ansari and Z. Zhao, *Faraday Discussions*, 2012, **154**, 9-27. 10.1039/C1FD00112D.
2. T. Tamura, K. Yoshida, T. Hachida, M. Tsuchiya, M. Nakamura, Y. Kazue, N. Tachikawa, K. Dokko and M. Watanabe, *Chemistry Letters*, 2010, **39**, 753-755. 10.1246/cl.2010.753.
3. C. Arbizzani, M. Biso, D. Cericola, M. Lazzari, F. Soavi and M. Mastragostino, *Journal of Power Sources*, 2008, **185**, 1575-1579. https://doi.org/10.1016/j.jpowsour.2008.09.016.
4. A. Balducci, R. Dugas, P. L. Taberna, P. Simon, D. Plée, M. Mastragostino and S. Passerini, *Journal of Power Sources*, 2007, **165**, 922-927. https://doi.org/10.1016/j.jpowsour.2006.12.048.
5. A. Eftekhari, Y. Liu and P. Chen, *Journal of Power Sources*, 2016, **334**, 221-239. https://doi.org/10.1016/j.jpowsour.2016.10.025.
6. A. Ray and B. Saruhan, *Materials*, 2021, **14**, 2942.
7. S. S. de Jesus and R. Maciel Filho, *Renewable and Sustainable Energy Reviews*, 2022, **157**, 112039. https://doi.org/10.1016/j.rser.2021.112039.
8. T. Mandai, K. Dokko and M. Watanabe, *The Chemical Record*, 2019, **19**, 708-722. https://doi.org/10.1002/tcr.201800111.
9. M. Watanabe, K. Dokko, K. Ueno and M. L. Thomas, *Bulletin of the Chemical Society of Japan*, 2018, **91**, 1660-1682. 10.1246/bcsj.20180216.
10. T. Mandai, K. Yoshida, K. Ueno, K. Dokko and M. Watanabe, *Physical Chemistry Chemical Physics*, 2014, **16**, 8761-8772. 10.1039/C4CP00461B.
11. T. Harte, B. Dharmasiri, G. S. Dobhal, T. R. Walsh and L. C. Henderson, *Physical Chemistry Chemical Physics*, 2023, DOI: 10.1039/D3CP04666D. 10.1039/D3CP04666D.
12. P. C. Marr and A. C. Marr, *Green Chemistry*, 2016, **18**, 105-128. 10.1039/C5GC02277K.
13. M. Safa, A. Chamaani, N. Chawla and B. El-Zahab, *Electrochimica Acta*, 2016, **213**, 587-593. https://doi.org/10.1016/j.electacta.2016.07.118.
14. M. A. B. H. Susan, T. Kaneko, A. Noda and M. Watanabe, *Journal of the American Chemical Society*, 2005, **127**, 4976-4983. 10.1021/ja045155b.
15. Z. Wang, H. Shi, W. Zheng, W. Sun, L. Zhao and W. Yuan, *Journal of Power Sources*, 2022, **524**, 231070. https://doi.org/10.1016/j.jpowsour.2022.231070.
16. T. Harte, B. Dharmasiri, P. Coia, D. J. Eyckens and L. C. Henderson, *Journal of Molecular Liquids*, 2024, DOI: https://doi.org/10.1016/j.molliq.2024.124689, 124689. https://doi.org/10.1016/j.molliq.2024.124689.
17. B. Dharmasiri, F. Stojcevski, K. A. S. Usman, S. Alex Qin, J. M. Razal, E. H. Doeven, P. S. Francis, T. U. Connell, Y. Yin, G. G. Andersson, A. Borkar and L. C. Henderson, *Chemical Engineering Journal*, 2023, **455**, 140778. https://doi.org/10.1016/j.cej.2022.140778.
18. A. Guerfi, M. Dontigny, P. Charest, M. Petitclerc, M. Lagacé, A. Vijh and K. Zaghib, *Journal of Power Sources*, 2010, **195**, 845-852. https://doi.org/10.1016/j.jpowsour.2009.08.056.
19. Shalu, V. K. Singh and R. K. Singh, *Journal of Materials Chemistry C*, 2015, **3**, 7305-7318. 10.1039/C5TC00940E.
20. N. Shirshova, A. Bismarck, S. Carreyette, Q. P. V. Fontana, E. S. Greenhalgh, P. Jacobsson, P. Johansson, M. J. Marczewski, G. Kalinka, A. R. J. Kucernak, J. Scheers, M. S. P. Shaffer, J. H. G. Steinke and M. Wienrich, *Journal of Materials Chemistry A*, 2013, **1**, 15300-15309. 10.1039/C3TA13163G.

21. M. I. Hossain and G. J. Blanchard, *The Journal of Physical Chemistry Letters*, 2023, **14**, 2731-2735. 10.1021/acs.jpclett.3c00329.
22. M. I. Hossain, H. Wang, L. Adhikari, G. A. Baker, A. Mezzetta, L. Guazzelli, P. Mussini, W. Xie and G. J. Blanchard, *The Journal of Physical Chemistry B*, 2024, **128**, 1495-1505. 10.1021/acs.jpcb.3c07967.
23. N. Hameed, D. J. Eyckens, B. M. Long, N. V. Salim, J. C. Capricho, L. Servinis, M. De Souza, M. D. Perus, R. J. Varley and L. C. Henderson, *ACS Applied Polymer Materials*, 2020, **2**, 2651-2657. 10.1021/acsapm.0c00257.
24. S. Grecu, M. Roggenbuck, A. Opitz and W. Brütting, *Organic electronics*, 2006, **7**, 276-286.
25. Y. Yoshimura, T. Takekiyo, Y. Imai and H. Abe, *The Journal of Physical Chemistry C*, 2012, **116**, 2097-2101. 10.1021/jp205314f.
26. Y. Yoshimura, H. Abe, Y. Imai, T. Takekiyo and N. Hamaya, *The Journal of Physical Chemistry B*, 2013, **117**, 3264-3269. 10.1021/jp400341r.
27. A. Porras-Vazquez, L. Martinie, P. Vergne and N. Fillot, *Physical Chemistry Chemical Physics*, 2018, **20**, 27280-27293. 10.1039/C8CP04620D.
28. T. Takekiyo and Y. Yoshimura, *The Journal of Physical Chemistry B*, 2020, **124**, 7659-7667. 10.1021/acs.jpcb.0c04954.
29. L. Su, M. Li, X. Zhu, Z. Wang, Z. Chen, F. Li, Q. Zhou and S. Hong, *The Journal of Physical Chemistry B*, 2010, **114**, 5061-5065. 10.1021/jp912191z.
30. T. Morita, M. Ushio, K. Kanoh, E. Tanaka and K. Nishikawa, *Japanese Journal of Applied Physics*, 2012, **51**, 076703. 10.1143/JJAP.51.076703.
31. O. Y. Fajardo, F. Bresme, A. A. Kornyshev and M. Urbakh, *The Journal of Physical Chemistry Letters*, 2015, **6**, 3998-4004. 10.1021/acs.jpclett.5b01802.
32. F. Borghi and A. Podestà, *Advances in Physics: X*, 2020, **5**, 1736949. 10.1080/23746149.2020.1736949.
33. R. S. Anaredy and S. K. Shaw, *The Journal of Physical Chemistry C*, 2018, **122**, 19731-19737. 10.1021/acs.jpcc.8b06608.
34. M. A. Gebbie, M. Valtiner, X. Banquy, E. T. Fox, W. A. Henderson and J. N. Israelachvili, *Proceedings of the National Academy of Sciences*, 2013, **110**, 9674-9679. doi:10.1073/pnas.1307871110.
35. R. Atkin, N. Borisenko, M. Drüschler, F. Endres, R. Hayes, B. Huber and B. Roling, *Journal of Molecular Liquids*, 2014, **192**, 44-54. https://doi.org/10.1016/j.molliq.2013.08.006.
36. S. Bovio, A. Podestà, C. Lenardi and P. Milani, *The Journal of Physical Chemistry B*, 2009, **113**, 6600-6603. 10.1021/jp9022234.
37. D. M. Markiewitz, Z. Goodwin, M. McEldrew, J. P. de Souza, X. Zhang, R. M. Espinosa-Marzal and M. Z. Bazant, *Faraday Discussions*, 2024.
38. D. Wang, Z. Wang, W. Liang, Y. Han, Y. Zhao, Y. Lv, L.-Y. Shi and S. Yuan, *Materials Chemistry Frontiers*, 2023.
39. S. Lin, L. Xu, A. Chi Wang and Z. L. Wang, *Nature communications*, 2020, **11**, 399. 10.1038/s41467-019-14278-9.
40. W. Kong, P. Cao, X. He, L. Yu, X. Ma, Y. He, L. Lu, X. Zhang and Y. Deng, *RSC Advances*, 2014, **4**, 19356-19361. 10.1039/C4RA00629A.
41. G. Selleri, F. Poli, R. Neri, L. Gasperini, C. Gualandi, F. Soavi and D. Fabiani, *Journal of Energy Storage*, 2023, **60**, 106660. https://doi.org/10.1016/j.est.2023.106660.
42. Y. Yu, Y. Shi, H. Kurita, Y. Jia, Z. Wang and F. Narita, *Composites Part A: Applied Science and Manufacturing*, 2023, **172**, 107587. https://doi.org/10.1016/j.compositesa.2023.107587.
43. R. Harnden, D. Carlstedt, D. Zenkert and G. Lindbergh, *ACS Applied Materials & Interfaces*, 2022, **14**, 33871-33880. 10.1021/acsami.2c08375.

Data Availability Statement

The raw data is available via our university repository.

Ž. Simon, B. Dharmasiri, T. Harte, Timothy, P. C. Sherrell, L. C. Henderson, 2024, Deakin University Research Repository, DOI: https://doi.org/10.26187/deakin.c.7362889